PERGAMON

International Journal of Heat and Mass Transfer 41 (1998) 4195–4204

International Journal of HEAT and MASS TRANSFER

Pulsed electromagnetic heating of microparticles

John F. Widmann*, E. James Davis†

Department of Chemical Engineering, University of Washington, Seattle, WA 98195-1750, U.S.A.

Received 8 September 1997; in final form 20 March 1998

Abstract

The application of pulsed heating by a laser beam to determine the thermal properties of microparticles is explored. Two problems are analyzed: (i) spatially uniform heating of the surface of an absorbing microsphere, and (ii) non-uniform surface heating based on Mie theory computations of the electromagnetic energy source. A parametric study shows that the spatially uniform heating model is sufficient when the thermal conductivity of the microparticle is sufficiently large or the Biot number is sufficiently low, but a more rigorous model is needed to predict the temperature distribution with the microsphere for lower thermal conductivity materials. The resulting analytical solutions are compared with previously published experiments involving infrared heating of single spherocarb particles and are shown to be in good agreement with time-dependent surface temperature measurements.

Nomenclature

a particle radius
$A_{mn}(\tau)$ time-dependent function
Bi composite Biot number
C specific heat
$\mathbf{E}, \mathbf{E}^*$ electric vector and its complex conjugate
$f(\tau)$ pulse function
h_c conduction/convection heat transfer coefficient
h_r radiation heat transfer coefficient
I_{inc} intensity of the incident laser beam
$J_p(z)$ Bessel function of the first kind of order p
m_{12} refractive index ratio
n order of the Legendre polynomial
N refractive index
N_{mn} norm of the eigenfunction, $X_{mn}(x)$
p order of the Bessel function
$P_n(\eta)$ Legendre polynomial of order n
$Q(r, \theta, \phi)$ heat source function
r radial coordinate
$S(x, \eta, \tau)$ nondimensional source function
t time
T temperature
U, W dimensionless temperatures
x dimensionless radial coordinate
X size parameter
$X_{mn}(x)$ eigenfunctions.

Greek symbols

α_r absorptivity of the particle
β dimensionless irradiance
γ_{mn} eigenvalues
ε_r emissivity of the particle
$\eta = \cos\theta$ independent angular variable
θ polar angle
κ thermal conductivity
λ_{inc} wavelength of the incident laser beam
λ_m eigenvalues
μ magnetic permeability
ρ density
σ the Stefan–Boltzman constant
τ dimensionless time
ϕ azimuthal angle.

Subscripts

1 particle property
2 surrounding gas property
c refers to conduction or convection
inc incident beam property
r refers to electromagnetic radiation.

* Current address: National Institute of Standards and Technology, High Temperature Processes Group, Bldg 221, Rm B312, Gaithersburg, MD 20899, U.S.A.

† Author to whom correspondence should be addressed.

0017–9310/98 $19.00
PII: S0017–9310(98)00126–4

1. Introduction

Particles with sizes in the range 1–200 μm are encountered in the atmosphere and produced in a number of processes. Of particular interest here are carbonaceous particles associated with combustion processes. The thermal and radiative properties of such microparticles can be measured by single particle experiments in which a charged microparticle is levitated in an electrodynamic balance (EDB) and illuminated with a laser beam. The principles and applications of the EDB have been surveyed by Davis [1, 2]. Spjut et al. [3] at MIT introduced the electrodynamic thermogravimetric analyzer (EDTGA) for the study of carbonaceous particles, and the MIT group performed a variety of investigations reviewed by Bar-Ziv et al. [4]. These include particle temperature measurements by infrared pyrometry and transient heating experiments [5]. Bar-Ziv and Sarofim [6] provided an additional review of the literature associated with particle heating in an EDB, including the effects of microparticle properties on the electromagnetic heat source function.

Monazam et al. [7] and Monazam and Maloney [8] at the Morgantown Energy Technology Center (METC) adapted the techniques of Spjut and his coworkers to determine heat capacities, temperatures and absorptivities of single carbon particles by means of pulsed heating experiments. A levitated particle with a diameter of order 100 μm was illuminated from two sides using a CO_2 laser (10.6 μm wavelength) with a repetition rate of 100 Hz and a pulse duration of 3 ms. The particle temperature was determined from measurements of the radiant emissive power of the particle using Planck's distribution law for the monochromatic radiant emission intensity.

The time-dependent temperature distribution in the microsphere was modeled by assuming that the heat flux associated with the electromagnetic radiation is uniform over the surface of the sphere. That is, the heat source was treated as a boundary condition rather than as an electromagnetic heat source within the sphere. Convective and radiative heat losses were included in the surface boundary condition, but for the conditions of the experiments gas phase conduction was the dominant heat loss. They solved the governing unsteady state heat conduction equation numerically, and performed parametric studies, comparing predicted surface temperatures with measured temperatures. The authors recognized that the use of a spatially uniform energy flux at the surface is an approximation that may not be valid for other materials with physical and optical properties that differ from carbon.

It was the objective of this work to develop a more rigorous analysis of unsteady state heating of a sphere by electromagnetic radiation, taking into account a spatially-dependent surface energy flux based on Mie theory. The analysis of the METC group is recovered as a special case of a more general formulation.

2. Uniform surface heating

The governing conduction equation and auxiliary conditions used by Monazam and his coworkers are

$$\rho_1 C_1 \frac{\partial T}{\partial t} = \kappa_1 \frac{1}{r^2}\frac{\partial}{\partial r}\left(r^2 \frac{\partial T}{\partial r}\right) \tag{1}$$

$$T(r,0) = T_0 \tag{2}$$

$$\frac{\partial T}{\partial r}(0,t) = 0 \tag{3}$$

and

$$\kappa_1 \frac{\partial T}{\partial r}(a,t) = \frac{1}{2}\alpha_r I_{inc}(t) - \{h_c[T(a,t)-T(\infty,t)] + \sigma\varepsilon_r[T^4(a,t)-T^4(\infty,t)]\}. \tag{4}$$

The incident intensity in boundary condition (4) is divided by two because the laser beam was split to heat the particle from two sides.

Monazam et al. solved this system of equations numerically, but for the conditions used in their experiments an approximate analytical solution can be obtained. This is accomplished by writing the approximation

$$T^4(a,t) - T_m^4 \cong [T_\infty^2(a,\infty)+T_\infty^2][T_m(a,\infty)+T_\infty][T(a,t)-T_\infty] \tag{5}$$

in which $T_m(a,\infty)$ is the mean surface temperature at large times, which can be computed by solving the energy balance,

$$0 = \frac{0.3}{2}\alpha_r I_{inc} - h_c[T_m(a,\infty)-T_\infty] - \sigma\varepsilon_r[T_m^4(a,\infty)-T_\infty^4]. \tag{6}$$

Here it is assumed that the heat flux averaged over one cycle is zero at large times, and that the electromagnetic energy was applied during 30% of the cycle which corresponds to the experiments of Monzama et al. Thus, using the linear approximation for the radiation heat loss, boundary condition (4) approximates to

$$\kappa_1 \frac{\partial T}{\partial r}(a,t) = \frac{1}{2}\alpha_r I_{inc}(t) - (h_c + h_r)[T(a,t)-T(\infty,t)] \tag{7}$$

in which

$$h_r = [T_m^2(a,\infty)+T_\infty^2][T_m(a,\infty)+T_\infty]. \tag{8}$$

As considered by Monazam et al., the heat transfer coefficient, h_c, is κ_2/a for a stagnant gas and for low gas Peclet numbers. For their conditions, h_r was less than 10% of h_c, so the linearization should be accurate at later times. The heat loss at early times is overestimated by this approximation because h_r is overestimated by using

the asymptotic mean surface temperature. Thus, it can be anticipated that the analytical solution developed using approximation (5) will underpredict the temperature at small times.

Defining nondimensional variables and parameters by

$$U(x,\tau)=\frac{T-T_0}{T_0},\quad x=\frac{r}{a},$$
$$\tau=\frac{\kappa_1}{\rho_1 C_1}\frac{t}{a^2},\quad Bi=\frac{(h_c+h_r)a}{\kappa_1}, \tag{9}$$

the boundary value problem becomes

$$\frac{\partial U}{\partial\tau}=\frac{1}{x^2}\frac{\partial}{\partial x}\left(x^2\frac{\partial U}{\partial x}\right) \tag{10}$$

$$U(x,0)=0,\quad \frac{\partial U}{\partial x}(0,\tau),\quad \frac{\partial U}{\partial x}(1,\tau)=\beta f(\tau)-Bi\,U(1,\tau). \tag{11}$$

Here β is the dimensionless electromagnetic energy flux defined by

$$\beta=\frac{a\alpha_r I_{inc}}{2\kappa_1 T_0} \tag{12}$$

and the normalized pulse function, $f(\tau)$, is unity for the first 3 ms of a pulse and zero for the next 7 ms of each pulse for the conditions of Monazam et al.

The solution of this system of equations is

$$U(x,\tau)=2\beta(1-Bi)\sum_{n=1}^{\infty}\frac{\sin\lambda_n}{(\sin^2\lambda_n-Bi)}\frac{\sin\lambda_n x}{x}\times\int_0^{\tau}f(\tau')\exp\left[-\lambda_n^2(\tau-\tau')\right]d\tau' \tag{13}$$

where the eigenvalues satisfy the transcendental equation

$$\tan\lambda_n=\frac{\lambda_n}{(1-Bi)}. \tag{14}$$

Carslaw and Jaeger [9] tabulated some of the eigenvalues based on equation (14) for a number of values of $(1-Bi)$.

The dimensionless surface temperature becomes

$$U(1,\tau)=2\beta(1-Bi)\sum_{n=1}^{\infty}\frac{\sin^2\lambda_n}{(\sin^2\lambda_n-Bi)}\times\int_0^{\tau}f(\tau')\exp\left[-\lambda_n^2(\tau-\tau')\right]d\tau'. \tag{15}$$

This result is compared with the numerical solution of Monazam and Maloney in Fig. 1. The physical parameters they used are $a=70$ μm, $\alpha_r=\varepsilon_r=0.85$, $I_{inc}=4.50$ MW m^{-2}, $\kappa_1=1.675$ W m^{-1} K^{-1}, $\kappa_2=0.048$ W m^{-1} K^{-1}, $C_1=1466$ J kg^{-1} K^{-1}, and $\rho_1=1050$ kg m^{-3}. The Biot number corresponding to their conditions is 0.032. The agreement is excellent at later times, and during the transient period when the time-averaged temperature changes, the analytical solution predicts temperatures only slightly lower than the numerical solution.

Monazam et al. used the same physical parameters as Monazam and Maloney to match theory and experiment except that they used $a=65$ μm and $C_1=1675$ J kg^{-1} K^{-1}, which corresponds to $Bi=0.031$. They did not report the value of α_r used, but they did state that their experimental results were consistent with values of α_r between 0.80 and 0.85. An expanded graph of their experimental results and our solution for the asymptotic region, in which the time-averaged surface temperature is constant, is presented in Fig. 2. Our solution is based upon an assumed value of $\alpha_r=0.85$. A more detailed comparison between theory and experiment is shown in Fig. 3 for one cycle in the asymptotic region. The agreement is very good, indicating that the best-fit parameters selected by Monazam and Maloney are consistent with their model of uniform surface heating.

3. Spatially nonuniform heating

The assumption of uniform surface heating is highly questionable when the thermal conductivity of the particle is not as large as that of carbon. A high thermal conductivity leads to small temperature gradients within the particle, and temperature variations associated with nonuniform heating can be expected to be smaller than for low-conductivity materials. The problem of plane wave electromagnetic heating of a sphere is described by Mie theory, and the treatise by Bohren and Huffman [9] provides details of Mie theory. The internal heat generation function for an absorbing sphere is

$$Q(r,\theta,\phi)=\frac{4\pi I_{inc}\,\mathrm{Re}\,[N_1]\,\mathrm{Im}\,[N_1]}{\lambda_{inc}}\frac{\mu_2}{\mu_1}\frac{\mathbf{E}\cdot\mathbf{E}^*}{E_{inc}^2}. \tag{16}$$

The radial, polar and azimuthal components of the electric vector at any point within the sphere are given by Bohren and Huffman in terms of the internal scattering coefficients and radial and polar eigenfunctions, and the reader can refer to that source for details. For a homogeneous sphere the internal electric field is governed by the size parameter, $X=2\pi aN_2/\lambda_{inc}$, and the relative refractive index, $m_{12}=N_1/N_2$.

Greene et al. [11] computed a number of source functions for various complex refractive indices and various size parameters, showing that the source function is very sensitive to both parameters. They presented normalized source functions for size parameters from 0.5–20.

Allen et al. [12] analyzed the problem of steady state one-sided heating of an absorbing microsphere using a Green's function solution to determine the temperature distribution within the sphere. They did not include the radiation boundary condition but used the heat source given by equation (16). Foss and Davis [13] extended the solution to unsteady state heat transfer by numerical computation, finding that significant temperature gradients arise with one-sided heating. Both Allen et al. and Foss and Davis computed source functions, $Q(r,\theta,\phi)$, for

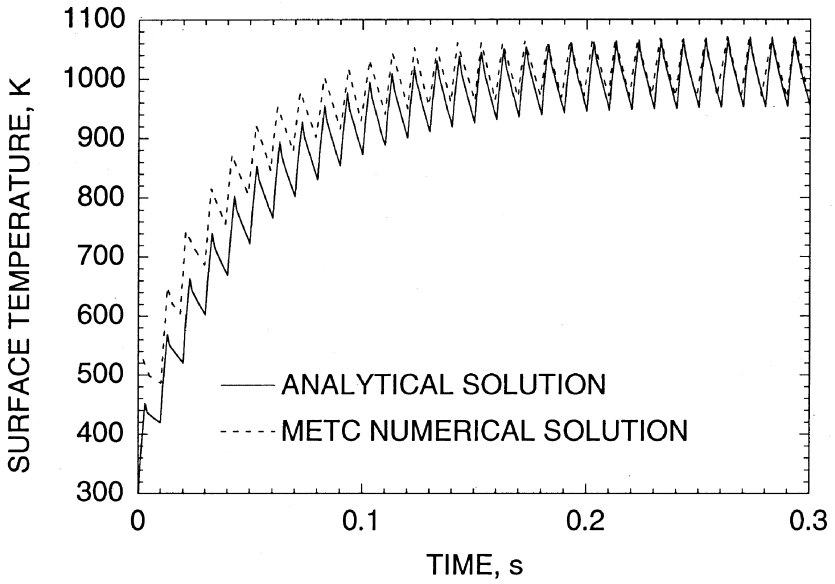

Fig. 1. A comparison between the numerical solution of Monazam and Maloney and equation (15) for $Bi = 0.032$.

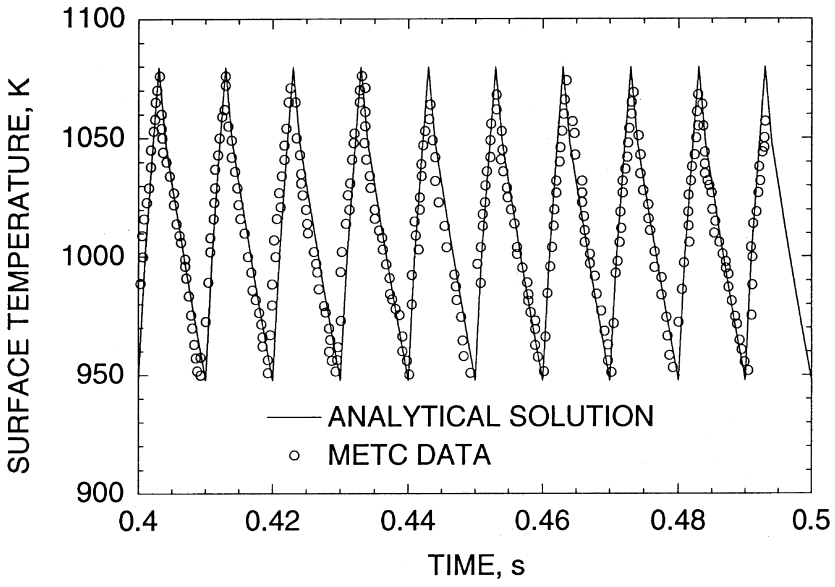

Fig. 2. A comparison between equation (15) and the data of Monazam et al. in the asymptotic region.

carbonaceous spheres having complex refractive index $N = 5.0 + i4.0$ at a laser wavelength of 10.6 μm.

For the 140 μm diameter sphere of Monazam and Maloney, $X = 41.498$. Using a refractive index of $N = 5.0 + i4.0$, we computed the source function presented in Fig. 4 for one-sided heating. Due to the strong absorption of electromagnetic energy, the source is concentrated near the surface. Our computations indicate that all of the energy absorption is confined to the outer 2% of the sphere, that is, to the region $x = r/a > 0.98$, and the source function is nearly independent of azimuthal angle ϕ. The result shown in Fig. 4 is qualitatively similar to those obtained by Greene et al. for the largest size parameter used by them.

The pulsed heating problem can now be solved using a source function such as that depicted in Fig. 4 or as an equivalent surface source problem. For two-sided heating, the shape of the source function, considered as a

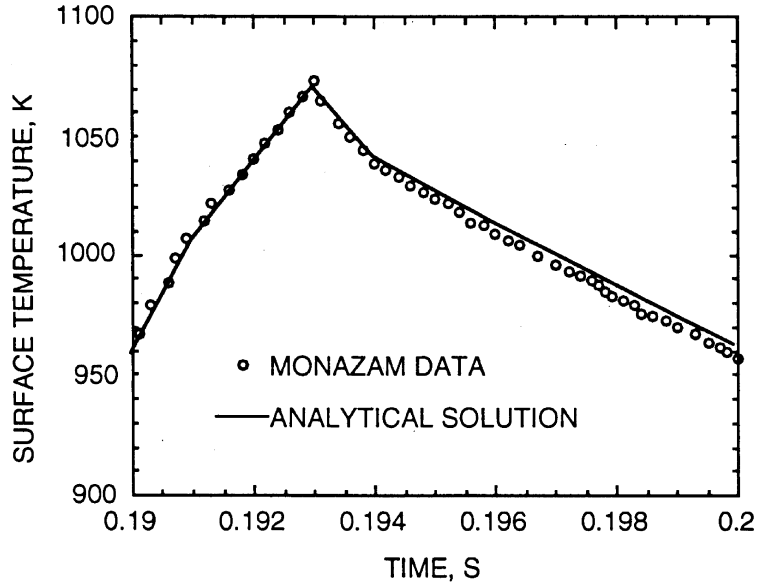

Fig. 3. A comparison between the data of Monazam et al. for one cycle and equation (15).

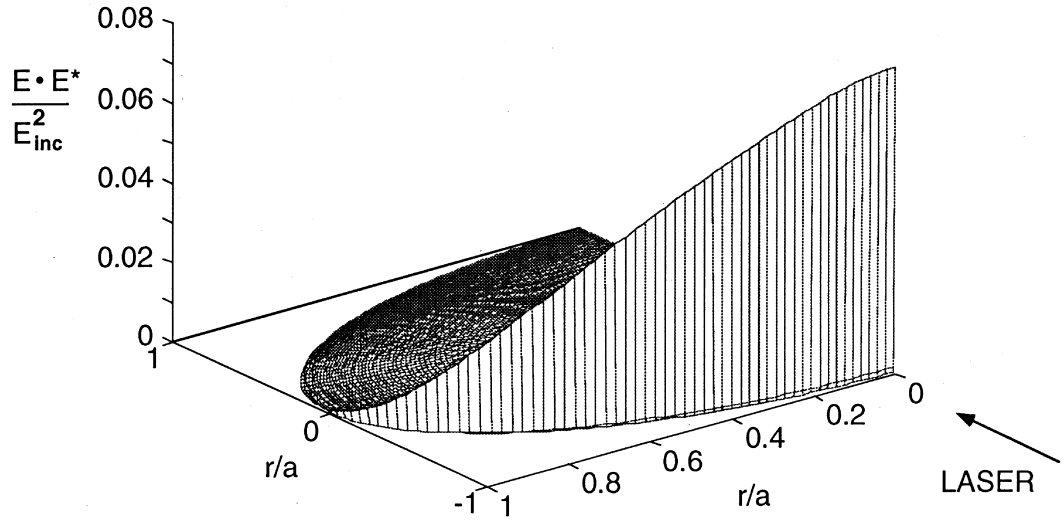

Fig. 4. The electromagnetic source in the half-sphere computed from Mie theory for one-sided heating.

surface source, can be approximated by the intensity distribution

$$I(a,\theta) = I_{\max}\cos^2\theta \tag{17}$$

where $I_{\max}$ is the intensity at $\theta = 0, 180^\circ$, and θ is measured from the direction of propagation of one of the laser beams. If I_{inc} is the laser intensity prior to beam-splitting, $I_{\max} = 3I_{\text{inc}}/2$ for the same energy absorption over the entire surface as in the previous case of uniform heating. The normalized intensity distribution, $I(a,\theta)/I_{\max}$, described by equation (17) is compared with the normalized electric field strength at the surface, $\mathbf{E}(a,\theta)\cdot\mathbf{E}^*(a,\theta)/\mathbf{E}(a,0)\cdot\mathbf{E}^*(a,0)$, in Fig. 5. The cosine-squared distribution is seen to be in very good agreement with the rigorous surface distribution function computed from Mie theory.

When the angular dependence of the temperature distribution is considered the nondimensional governing equations become

$$\frac{\partial U}{\partial \tau} = \frac{1}{x^2}\frac{\partial}{\partial x}\left(x^2\frac{\partial U}{\partial x}\right) + \frac{1}{x^2}\frac{\partial}{\partial \eta}\left[(1-\eta^2)\frac{\partial U}{\partial \eta}\right] \tag{18}$$

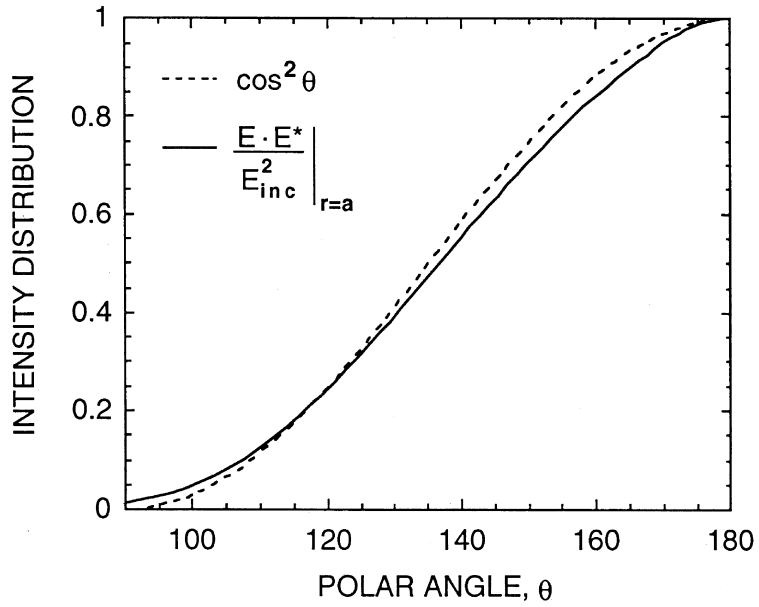

Fig. 5. The normalized surface source computed from Mie theory compared with the approximation, equation (17).

$$U(x,0)=0,\quad \frac{\partial U}{\partial x}(0,\tau)=0,$$

$$\frac{\partial U}{\partial x}(1,\tau)=3\beta f(\tau)\eta^2-Bi\,U(1,\tau). \tag{19}$$

The solution of this problem can be obtained by writing $U(x,\eta,\tau)$ as a superposition of two functions,

$$U(x,\eta,\tau)=\frac{3\beta}{(2+Bi)}x^2f(\tau)\eta^2+W(x,\eta,\tau). \tag{20}$$

The first function on the right-hand side of equation (20) satisfies the inhomogeneous boundary condition at $x=1$, and $W(x,\eta,\tau)$ satisfies the inhomogeneous partial differential equation

$$\frac{\partial W}{\partial\tau}=\frac{1}{x^2}\frac{\partial}{\partial x}\left(x^2\frac{\partial W}{\partial x}\right)+\frac{1}{x^2}\frac{\partial}{\partial\eta}\left[(1-\eta^2)\frac{\partial W}{\partial\eta}\right]-S(x,\eta,\tau) \tag{21}$$

with auxiliary conditions,

$$W(x,\eta,0)=-\frac{3\beta}{(2+Bi)}x^2f(0)\eta^2,$$

$$\frac{\partial W}{\partial x}(0,\eta,\tau)=0,\quad \frac{\partial W}{\partial x}(1,\tau)=-Bi\,W(1,\eta,\tau). \tag{22}$$

The source term $S(x,\eta,\tau)$ is

$$S(x,\eta,\tau)=-\frac{3\beta}{(2+Bi)}\left\{\left[6f(\tau)-x^2\frac{\mathrm{d}f}{\mathrm{d}\tau}\right]\eta^2+2f(\tau)(1-3\eta)^2)\right\}. \tag{23}$$

We note that the problem involving $W(x,\eta,\tau)$ is the equivalent of the source term problem in which $-S(x,\eta,\tau)$ in equation (21) is replaced by the volumetric source $\rho Ca^2Q(r,\theta,\phi)/\kappa_1T_0$ with $Q(r,\theta,\phi)$ given by equation (16), and $W(x,\eta,0)=0$ based on the initial condition that $T=T_0$.

Since $P_0(\eta)=1$, and $P_2(\eta)=(3\eta^2/2-1/2)$, where $P_n(\eta)$ is the Legendre polynomial of order n, we look for a solution of the form

$$W(x,\eta,\tau)=\sum_{m=1}^{\infty}A_{m0}(\tau)X_{m0}(x)P_0(\eta)+\sum_{m=1}^{\infty}A_{m2}(\tau)X_{m2}(x)P_2(\eta) \tag{24}$$

where the eigenfunctions are

$$X_{m0}(x)=\frac{1}{\sqrt{x}}J_{1/2}(\gamma_{m0}x)=\sqrt{\frac{2}{\pi\gamma_{m0}}}\frac{\sin\gamma_{m0}x}{x} \tag{25}$$

and

$$X_{m2}(x)=\frac{1}{\sqrt{x}}J_{5/2}(\gamma_{m2}x)=\sqrt{\frac{2}{\pi\gamma_{m2}}}\times\left[\left(\frac{3}{\gamma_{m2}^2x^3}-\frac{1}{x}\right)\sin\gamma_{m2}x-\frac{3}{\gamma_{m2}x^2}\cos\gamma_{m2}x\right]. \tag{26}$$

Here $J_p(z)$ is the Bessel function of the first kind of order p, and $p=(1/2)\sqrt{1+4n(n+1)}$ for $n=0$ and 2. The eigenvalues γ_{m0} satisfy the same transcendental equation as λ_n, equation (14), and eigenvalues γ_{m2} satisfy

$$\tan\gamma_{m2}=\frac{\gamma_{m2}^3-3(3-Bi)\gamma_{m2}}{(4-Bi)\gamma_{m2}^2-3(3-Bi)}. \tag{27}$$

Substituting these results into equation (21) and the initial condition, and applying orthogonality of the eigenfunctions, one obtains

$$W(x,\eta,\tau) = \frac{3\beta}{(2+Bi)}\sum_{m=1}^{\infty}\left\{-\frac{I_2}{3}f(\tau) \quad +\left(2I_1+\frac{\gamma_{m0}^2}{3}I_2\right)\right.$$
$$\left.\times\int_0^{\tau} f(\tau')\,\mathrm{e}^{-\gamma_{m0}^2(\tau-\tau')}\,\mathrm{d}\tau'\right\}\frac{X_{m0}(x)}{N_{m0}^2}$$
$$-\frac{2\beta}{(2+Bi)}\left(\frac{3}{2}\eta^2-\frac{1}{2}\right)\sum_{m=1}^{\infty} I_3\left\{f(\tau)-\gamma_{m2}^2\right.$$
$$\left.\times\int_0^{\tau} f(\tau')\,\mathrm{e}^{-\gamma_{m2}^2(\tau-\tau')}\,\mathrm{d}\tau'\right\}\frac{X_{m2}(x)}{N_{m2}^2}. \tag{28}$$

Here the norms, N_{mn}, of the eigenfunctions are

$$N_{m0}^2 = \frac{(\gamma_{m0}-\sin\gamma_{m0}\cos\gamma_{m0})}{\pi\gamma_{m0}^2} \tag{29}$$

and

$$N_{m2}^2 = \frac{1}{2}[J_{5/2}^2(\gamma_{m2})+J_{3/2}^2(\gamma_{m2})]-\frac{5}{2\gamma_{m2}}J_{5/2}(\gamma_{m2})J_{3/2}(\gamma_{m2}). \tag{30}$$

The integrals I_1, I_2 and I_3 are defined by

$$I_1 = \int_0^1 x'^2 X_{m0}(x')\,\mathrm{d}x' = \sqrt{\frac{2}{\pi\gamma_{m0}^5}}(\sin\gamma_{m0}-\lambda_{m0}\cos\gamma_{m0}) \tag{31}$$

$$I_2 = \int_0^1 x'^4 X_{m0}(x')\,\mathrm{d}x' = \sqrt{\frac{2}{\pi\gamma_{m0}^9}}[(3\gamma_{m0}^2-6)\sin\lambda_{m0} - (\gamma_{m0}^3-6\gamma_{m0}^2)\cos\gamma_{m0}] \tag{32}$$

and

$$I_3 = \int_0^1 x'^4 X_{m2}(x')\,\mathrm{d}x' = \frac{1}{\gamma_{m2}}J_{7/2}(\gamma_{m2}). \tag{33}$$

Finally, the nondimensional temperature distribution $U(x,\eta,\tau)$ is given by equation (20) with $W(x,\eta,\tau)$ given by equation (28), and the nondimensional surface temperature reduces to

$$U(1,\eta,\tau) = \frac{\beta}{(2+Bi)}\left\{[1-f(\tau)]\right.$$
$$+\sum_{m=1}^{\infty}(6I_1+\gamma_{m0}^2I_2)\frac{X_{m0}(1)}{N_{m0}^2}\int_0^{\tau} f(\tau')\,\mathrm{e}^{-\gamma_{m0}^2(\tau-\tau')}\,\mathrm{d}\tau'$$
$$\left.+(3\eta^2-1)\sum_{m=1}^{\infty}\gamma_{m2}^2I_3\frac{X_{m2}(1)}{N_{m2}^2}\int_0^{\tau} f(\tau')\,\mathrm{e}^{-\gamma_{m2}^2(\tau-\tau')}\,\mathrm{d}\tau'\right\}. \tag{34}$$

The last term in equation (34) shows explicitly the dependence of the surface temperature on polar angle since $\eta=\cos\theta$. The maximum surface temperatures can be expected to occur at $\theta = 0^\circ$ and 180°. We note that when $\eta^2 = 1/3$ (or $\theta = 54.34^\circ$ and 125.26°) the last term in equation (34) vanishes.

The surface temperatures at $\theta = 0$ and 90° calculated using equation (34) are plotted in Fig. 6 as a function of time from $t = 0$–0.3 s, which covers the transient period. The physical parameters used by Monazam and Maloney have been used for the computations. Even for the relatively low Biot number involved in these results the surface temperature varies nontrivially in the θ direction. The temporal temperature fluctuations at $\theta = 0^\circ$ range over 190 K at long times, and those at $\theta = 90^\circ$ range over 70 K. This is more clearly shown in Fig. 7 when the surface temperature in the asymptotic region is shown for $\theta = 0$, 30, 60 and 90°. Thus, relatively large temperature gradients in the θ-direction are encountered in the particle.

At larger Biot numbers (or smaller particle thermal conductivities) the angular variation in the surface temperature becomes even more significant. This is shown in Fig. 8 for $\theta = 0$ and 90° with $\kappa_1 = 0.167$ ($Bi = 0.320$). The other physical properties are those used by Monazam and Maloney. Note that large temperature fluctuations occur at $\theta = 0^\circ$ where the electromagnetic energy flux is a maximum, but the fluctuations at $\theta = 90^\circ$ are severely damped due to the low thermal conductivity of the particle. The large temperature gradients are more clearly observed in Fig. 9 which shows the surface temperature at $\theta = 0$ and 90° for one cycle. Unlike the case for the lower Bi number shown in Fig. 7 ($\kappa_1 = 1.67$, $Bi = 0.032$) in which the maximum temperatures at each angle are nearly in phase, the maximum temperature at $\theta = 90^\circ$ lags behind the maximum at $\theta = 0^\circ$ due to the lower thermal conductivity of the particle.

4. Discussion of results

The linearized theory developed above is valid provided that $h_c \gg h_r$, but as the laser intensity increases the linear approximation of equation (8) becomes inaccurate, and the nonlinear system must be solved numerically. For the conditions of Monazam and his coworkers the asymptotic mean surface temperature is 1015 K, $T_{max} = 1080$ K and $T_{min} = 950$ K from Fig. 2, which is based on no angular variations in the surface temperature. The radiation heat flux is given by

$$q_r = \sigma\varepsilon_r[T^4(a,\infty)-T_\infty^4], \tag{35}$$

which, for the conditions used to obtain Fig. 2, yields a flux based on the mean temperature of $q_r = 50.8\ \mathrm{kW\,m^{-2}\,K^{-1}}$. This should be compared with the conduction heat flux given by

$$q_c = \frac{\kappa_2}{a}[T(a,\infty)-T_\infty]. \tag{36}$$

Based on $T_m(a,\infty) = 1015$ K, $q_c = 531.7\ \mathrm{kW\,m^{-2}\,K^{-1}}$. The maximum and minimum radiation heat fluxes at

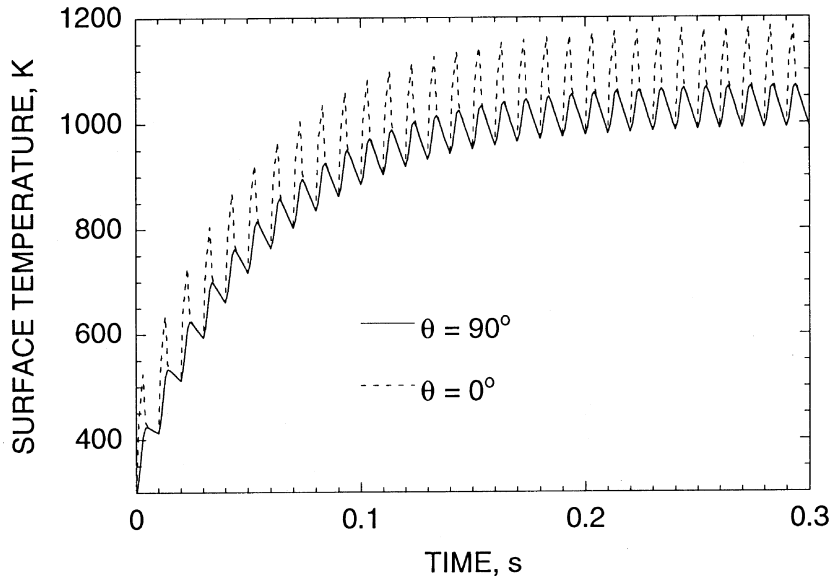

Fig. 6. The time-dependent surface temperature computed using equation (34) for $\theta = 0$ and 90° with $Bi = 0.032$.

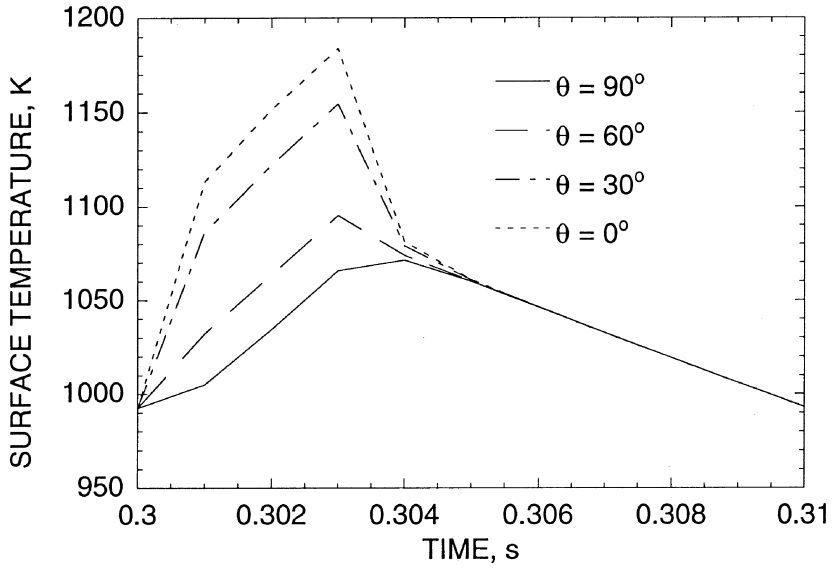

Fig. 7. The surface temperature for one cycle in the asymptotic region for $Bi = 0.032$ and various angles $\theta = 0$, 30, 60 and 90°.

large times are given by $q_{r,max} = 65.2$ kW m^{-2} K^{-1} and $q_{r,min} = 38.9$ kW m^{-2} K^{-1}. The corresponding conduction heat fluxes are $q_{c,max} = 579.7$ kW m^{-2} K^{-1} and $q_{c,min} = 483.7$ kW m^{-2} K^{-1}. The total heat fluxes become $q_{max} = 645.1$ kW m^{-2} K^{-1}, $q_{min} = 522.6$ kW m^{-2} K^{-1} and $q_m = 582.5$ kW m^{-2} K^{-1}. The radiation heat flux is seen to be less than 11% of the total heat flux at any surface temperature reached.

Neglecting angular variations in the surface temperature, the composite Biot numbers corresponding to these conditions are $Bi_{max} = 0.0319$, $Bi_{min} = 0.0310$, and $Bi_m = 0.0314$. Thus, the composite Biot number, which governs the heat loss, is nearly independent of the fluctuations in the surface temperature in this case, and the use of the asymptotic mean surface temperature to determine the radiation heat loss will be accurate. As I_{inc} increases, however, the linear approximation becomes invalid.

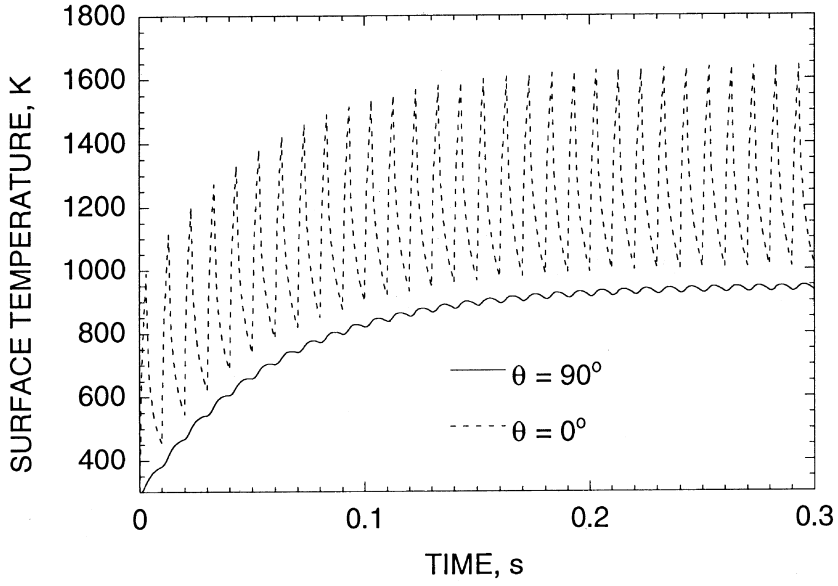

Fig. 8. The time-dependent surface temperature computed using equation (34) for $\theta = 0$ and 90° with $Bi = 0.320$.

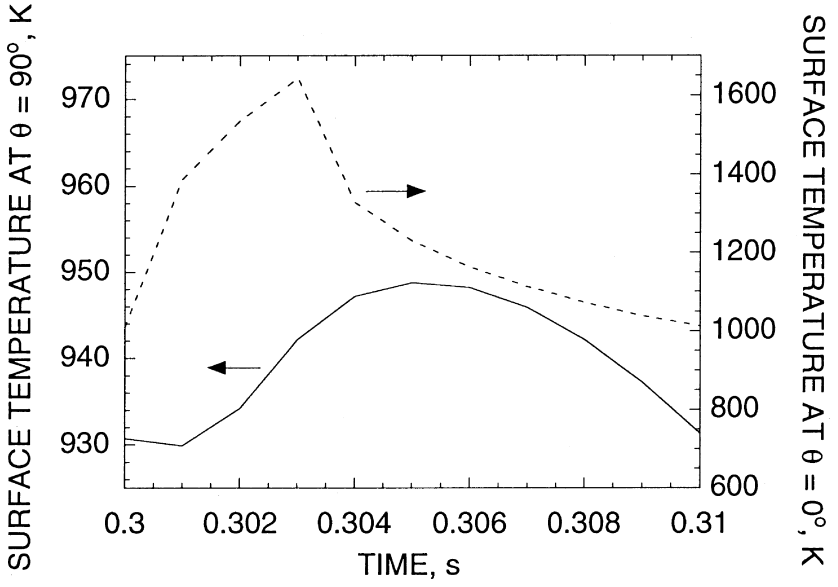

Fig. 9. The surface temperature for one cycle in the asymptotic region for $\theta = 0$ and 90° with $Bi = 0.320$.

When the more realistic model of the surface irradiation is applied, the surface temperature fluctuations increase, but again the local composite Biot numbers will not vary greatly provided that nonlinear effects are small. The analytical solution, equation (34), makes it possible to routinely carry out parametric studies to determine the best fit of the parameters to match experimental data. It was shown above that significant temperature gradients can result in the particle due to the non-uniform heating, and that even modest values of Bi can result in angular variations of the surface temperature that persist throughout the entire heating cycle.

The analysis developed here can be extended to one-sided heating, and one can expect very significant angular variations in the surface temperature when one-sided heating is applied. It is also possible to relax the assumption of surface heating by using the internal heat source computed from Mie theory to generalize the procedure

to any microsphere with a known size and complex refractive index.

Acknowledgments

The authors are grateful to NASA for Grant NAG-1837 which supported the research. They also acknowledge the preliminary computations of Matthew Tadd.

References

[1] E.J. Davis, Microchemical engineering: the chemistry and physics of the microparticle, in: J.L. Anderson (Ed.), Advances in Chemical Engineering, vol. 18, Academic Press, New York, 1992, pp. 1–94.
[2] E.J. Davis, A history of single aerosol particle levitation, Aerosol Sci. Technol. 26 (1997) 212–254.
[3] R.E. Spjut, E. Bar-Ziv, A.F. Sarofim, J.P. Longwell, Electrodynamic thermogravimetric analyzer, Rev. Sci. Instrum. 57 (1986) 1604–1610.
[4] E. Bar-Ziv, D.B. Jones, R.E. Spjut, D.R. Dudek, A.F. Sarofim, J.P. Longwell, Measurement of combustion kinetics of a single char particle in an electrodynamic thermogravimetric analyzer, Combust. Flame 75 (1989) 81–106.
[5] R.E. Spjut, A.F. Sarofim, J.P. Longwell, Laser heating and particle temperature measurement in an electrodynamic balance, Langmuir 1 (1985) 355–360.
[6] E. Bar-Ziv, A.F. Sarofim, The electrodynamic chamber: a tool for studying high temperature kinetics involving liquid and solid particles, Prog. Energy Combust. Sci. 17 (1991) 1–65.
[7] E.R. Monazam, D.J. Maloney, L.O. Lawson, Measurements of heat capacities, temperatures, and absorptivities of single particles in an electrodynamic balance, Rev. Sci. Instrum. 60 (1989) 3460–3465.
[8] E.R. Monazam, D.J. Maloney, Temperature transients associated with pulsed heating of single particles, J. Appl. Phys. 71 (1992) 2552–2559.
[9] H.S. Carslaw, J.C. Jaeger, Conduction of Heat in Solids, 2nd ed. Oxford University Press, Fair Lawn, NJ, 1959.
[10] C.F. Bohren, D.R. Huffman, Absorption and Scattering of Light by Small Particles, John Wiley and Sons, New York, 1983.
[11] W.M. Greene, R.E. Spjut, E. Bar-Ziv, A.F. Sarofim, J.P. Longwell, Photophoresis of irradiated spheres: absorption centers, Opt. Soc. Am. B 2 (1985) 998–1004.
[12] T.M. Allen, M.F. Buehler, E.J. Davis, Radiometric effects on absorbing microspheres, J. Colloid Interface Sci 142 (1991) 343–356.
[13] W.R. Foss, E.J. Davis, Transient laser heating of single solid microspheres, Chem. Eng. Comm. 152–153 (1996) 113–138.